JOURNAL OF GUIDANCE, CONTROL, AND DYNAMICS
Vol. 30, No. 4, July–August 2007

Orbital Rendezvous: When Is Autonomy Required?

David K. Geller*
Utah State University, Logan, Utah 84322

DOI: 10.2514/1.27052

The ability to control the relative motion of two orbiting spacecraft from the ground is approximately a function of four key parameters: relative state knowledge errors, maneuver execution errors, environment modeling errors, and the time delay between the execution of successive maneuvers. Based on these four parameters an assessment of the ground's capability to control relative position can be made and a minimum safe-approach distance can be determined. Approximate analytic expressions for minimum ground-controlled separations are presented and then validated with a detailed linear covariance analysis. The analytic expressions are shown to be accurate to within ±25%.

Nomenclature

D_{nav}	=	covariance of navigation state dispersions
D_{true}	=	covariance of true state dispersions
$\text{diag}(\mathbf{v})$	=	diagonal matrix with elements of vector $\mathbf{v}$ along the diagonal
$\mathbf{F}^i_{\text{grav}}$	=	gravitational force in an inertial coordinate frame
$I_{n\times n}$	=	identity matrix
$O_{m\times n}$	=	matrix of zeros
$\hat{P}$	=	flight computer covariance of navigation state error
P_{orb}	=	orbital period
P_{true}	=	true covariance of navigation state error
$\mathbf{p}_{\Delta v}$	=	impulsive actuator model parameters
$\mathbf{q}$	=	quaternion indicated by boldface q
$\mathbf{q}^a_b$	=	quaternion representing the orientation of the b frame with respect to the a frame
$\mathbf{q}^i_c$	=	quaternion representing the orientation of the chaser frame with respect to the inertial frame
$\mathbf{R}^{\text{LVLH}}$	=	position of chaser relative to an object centered rotating LVLH frame
$\mathbf{r}^i_c$	=	position of chaser in an inertial coordinate frame
$\mathbf{r}^i_o$	=	position of object in an inertial coordinate frame
$\mathcal{T}^a_b$	=	direction cosine matrix representing the orientation of the b frame with respect to the a frame
$\mathcal{T}^i_c$	=	direction cosine matrix representation of $\mathbf{q}^i_c$
$\mathbf{V}^{\text{LVLH}}$	=	velocity of chaser relative to an object centered rotating LVLH frame
$\mathbf{v}$	=	vector indicated by boldface type
$\mathbf{v}^a$	=	vector represented in coordinate frame a
$\mathbf{v}^i_c$	=	velocity of chaser in an inertial coordinate frame
$\mathbf{v}^i_o$	=	velocity of object in an inertial coordinate frame
$\mathbf{x}$	=	true states
$\hat{\mathbf{x}}$	=	flight computer navigation states
$\bar{\mathbf{x}}$	=	reference states
$\tilde{\mathbf{z}}_k$	=	measurements at time t_k
Δt	=	time between successive maneuvers
$\Delta\mathbf{v}^i_{\text{act}}$	=	actuator Δv in an inertial coordinate frame
$\delta\mathbf{e}$	=	true navigation error
$\delta\mathcal{T}(\boldsymbol{\epsilon})$	=	direction cosine matrix associated with a small rotation, $\delta\mathcal{T}(\boldsymbol{\epsilon}) \approx I - [\boldsymbol{\epsilon}\times]$
$\delta(t-t')$	=	Dirac delta function
$\delta\mathbf{x}$	=	true state dispersions
$\delta\hat{\mathbf{x}}$	=	navigation state dispersions
$\delta_{jj'}$	=	Kronecker delta function
$\boldsymbol{\epsilon}$	=	small rotation vector
$[\boldsymbol{\epsilon}\times]$	=	cross product matrix defined by the ordinary cross product $[\epsilon\times]\mathbf{v} = \boldsymbol{\epsilon}\times\mathbf{v}$
ω_{orb}	=	orbital frequency
$\hat{}$	=	parameters, variables, and functions associated with the flight algorithms
$\tilde{}$	=	measured values
$\bar{}$	=	reference values
$\otimes$	=	quaternion multiplication operator such that $\mathbf{q}^a_c = \mathbf{q}^b_c \otimes \mathbf{q}^a_b$ corresponds to the sequence of rotations $\mathcal{T}^a_c = \mathcal{T}^b_c\mathcal{T}^a_b$

Introduction

INTEREST in orbital rendezvous missions has been growing as witnessed by the recent design and/or development of XSS-11, DART (Demonstration of Autonomous Rendezvous Techniques), Orbital Express, and the Hubble Robotic Servicing and Deorbit Mission [1,2]. In the future there may be new satellite inspection and satellite servicing missions, lunar exploration missions, Mars sample and return missions, and perhaps a Titan sample and return mission, all of which will require some form of orbital rendezvous.

Without a human in the loop, it will be important to know when ground controllers can safely control the relative motion of two orbiting spacecraft, and when onboard autonomous systems are required. It is assumed that beyond some *safe-approach distance*, ground controllers have the ability to safely command and control the relative motion. Within this safe-approach distance, when close proximity operations are required, onboard autonomous systems must take over.

The objective of this paper is to determine and verify analytic expressions for the minimum ground-controlled safe-approach distance. From a guidance, navigation, and control (GNC) perspective, the minimum safe-approach distance is determined by four key parameters: 1) the time delay between successive ground-commanded maneuvers, 2) navigation error, 3) maneuver execution accuracy, and 4) environment modeling error. When these parameters are known, an estimate of the minimum safe-approach distance can be determined using simple expressions that will be derived and verified in this paper.

The model for the onboard and ground operations of a generic rendezvous mission is shown in Fig. 1. In this simplified picture, onboard measurement data are continuously downlinked to the ground. When the spacecraft is out of view, it is assumed that the data are stored onboard and downlinked at a later time. The ground processes the measurement data and estimates the relative state. At the proper time a maneuver command is computed and uplinked to the chaser where it is immediately executed. The ground continues to

Presented as Paper 6298 at the AIAA/AAS Astrodynamics Specialists Conference, Keystone, CO, 21–24 August 2006; received 4 August 2006; revision received 17 February 2007; accepted for publication 13 March 2007.

*Assistant Professor, Mechanical and Aerospace Engineering Department. Senior Member AIAA.

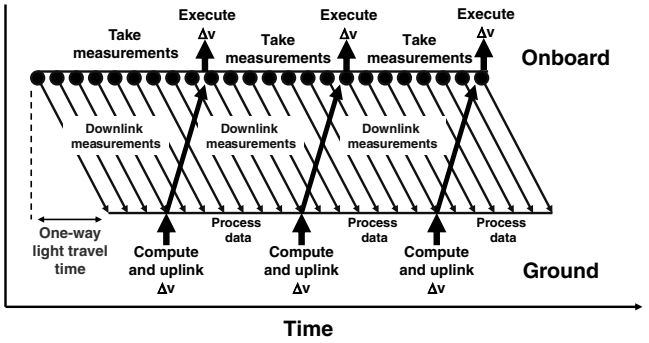

Fig. 1 A simple model for onboard and ground operations of a generic rendezvous mission.

process measurement data. The time between maneuvers is a key parameter in this analysis. It must take into account the light-travel time, communication outages, processing delays, and extra time to collect measurements after maneuvers. Overall, this ground operations model is ideal and subsequent calculations will represent an upper bound on ground control capabilities.

Three different rendezvous missions will be considered: 1) Mars orbit rendezvous for sample return, 2) low lunar orbit rendezvous for lunar exploration, and 3) geosynchronous orbit (GEO) rendezvous for satellite inspection and servicing. In each case, the active vehicle will be referred to as the chaser, and the passive vehicle (i.e., the orbiting sample, or a lunar surface access vehicle, or a geostationary satellite) will be referred to as the resident space object (RSO). For the Mars missions, the minimum separation distance will be relatively large due to communication interruptions and long round-trip light-travel times. For low lunar orbit rendezvous, the minimum ground-controlled separation distance will be smaller due to shorter light-travel times. For GEO missions, the potential to control two spacecraft in close proximity to each other from the ground exists if near real-time tracking data or relative position/velocity measurement data are available.

For each mission it is assumed that the chaser is station keeping at a specified distance from the RSO as shown in Fig. 2. In this figure, the vertical or radial direction, r bar, and the local horizontal in-plane direction, v bar, define a local–vertical local–horizontal (LVLH) frame. For each mission it is assumed that the chaser is station keeping in front of the RSO in the direction of the inertial velocity on or near the v bar. The 3-σ station-keeping dispersions, $3\sigma_{sk}$, for a ground-controlled spacecraft must be less than some specified fraction f of the downrange distance d to the RSO. If maneuvers cannot be computed, uplinked, and executed frequently enough to maintain $3\sigma_{sk} \leq fd$, an unsafe condition results, and an autonomous system must be introduced for quicker response time. Thus it is the 3-σ station-keeping dispersions that will determine the minimum ground-controlled safe-approach distance.

In the next section, two new analytical equations are derived for the chaser 3-σ station-keeping dispersions relative to the RSO as a function of navigation error, maneuver execution error, modeling error, and the time between maneuvers. The analytical results are shown to be very useful in determining minimum ground-controlled closest-approach distances. The following section provides detailed models for rendezvous dynamics, sensors, actuators, and flight algorithms. These models are then used to conduct a detailed linear covariance [3] analysis and to generate numerical results that will be compared to the analytical results. The Appendix presents the partial derivative used in the linear covariance analysis.

Simplified Analysis Using the Clohessy–Wiltshire Equations

The Clohessy–Wiltshire equations [4], also known as Hill's equations, can be written in the form

$$\begin{bmatrix} \mathbf{R}^{\mathrm{LVLH}}(t_0+\Delta t) \\ \mathbf{V}^{\mathrm{LVLH}}(t_0+\Delta t) \end{bmatrix} = \begin{bmatrix} \Phi_{rr}(\Delta t) & \Phi_{rv}(\Delta t) \\ \Phi_{vr}(\Delta t) & \Phi_{vv}(\Delta t) \end{bmatrix} \begin{bmatrix} \mathbf{R}^{\mathrm{LVLH}}(t_0) \\ \mathbf{V}^{\mathrm{LVLH}}(t_0)+\Delta\mathbf{v} \end{bmatrix} + \int_0^{\Delta t} \begin{bmatrix} \Phi_{rr}(\tau) & \Phi_{rv}(\tau) \\ \Phi_{vr}(\tau) & \Phi_{vv}(\tau) \end{bmatrix} \begin{bmatrix} 0 \\ \mathbf{a}_d \end{bmatrix} \mathrm{d}\tau \tag{1}$$

where we assume Δt is the time between maneuvers, $\Delta\mathbf{v}$ is the maneuver delta-v, and $\mathbf{a}_d$ is a random disturbance representing unmodeled differential accelerations due to solar radiation pressure, atmospheric drag, plume effects, and J_2 and higher-order gravity terms. If the x, y, and z components of $\mathbf{R}^{\mathrm{LVLH}}$ are altitude, downrange, and cross track, respectively, the above transition matrices are given by

$$\Phi_{rr}(\Delta t) = \begin{bmatrix} 4-3\cos(\omega_{\mathrm{orb}}\Delta t) & 0 & 0 \\ 6\sin(\omega_{\mathrm{orb}}\Delta t) - 6\omega_{\mathrm{orb}}\Delta t & 1 & 0 \\ 0 & 0 & \cos(\omega_{\mathrm{orb}}\Delta t) \end{bmatrix} \tag{2}$$

$$\Phi_{rv}(\Delta t) = \begin{bmatrix} \sin(\omega_{\mathrm{orb}}\Delta t)/\omega_{\mathrm{orb}} & 2\{1-\cos(\omega_{\mathrm{orb}}\Delta t)\}/\omega_{\mathrm{orb}} & 0 \\ 2\{\cos(\omega_{\mathrm{orb}}\Delta t)-1\}/\omega_{\mathrm{orb}} & 4\sin(\omega_{\mathrm{orb}}\Delta t)/\omega_{\mathrm{orb}} - 3\Delta t & 0 \\ 0 & 0 & \sin(\omega_{\mathrm{orb}}\Delta t)/\omega_{\mathrm{orb}} \end{bmatrix} \tag{3}$$

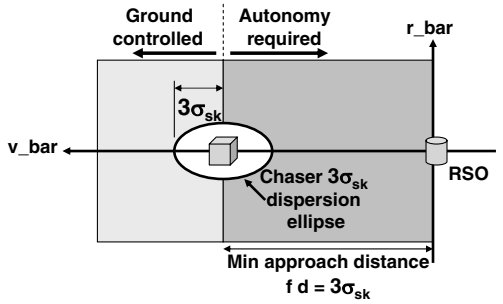

Fig. 2 The positions of the chaser and resident space object (RSO) in an RSO centered LVLH frame. The chaser is shown station keeping near the v bar. When the 3-σ station-keeping dispersions, $3\sigma_{sk}$, are equal to a specified fraction f of the distance d, the chaser is at a minimum ground-controlled safe-approach distance.

$$\Phi_{vr}(\Delta t) = \begin{bmatrix} 3\omega_{\mathrm{orb}}\sin(\omega_{\mathrm{orb}}\Delta t) & 0 & 0 \\ 6\omega_{\mathrm{orb}}\{\cos(\omega_{\mathrm{orb}}\Delta t)-1\} & 0 & 0 \\ 0 & 0 & -\omega_{\mathrm{orb}}\sin(\omega_{\mathrm{orb}}\Delta t) \end{bmatrix} \tag{4}$$

$$\Phi_{vv}(\Delta t) = \begin{bmatrix} \cos(\omega_{\mathrm{orb}}\Delta t) & 2\sin(\omega_{\mathrm{orb}}\Delta t) & 0 \\ -2\sin(\omega_{\mathrm{orb}}\Delta t) & 4\cos(\omega_{\mathrm{orb}}\Delta t)-3 & 0 \\ 0 & 0 & \cos(\omega_{\mathrm{orb}}\Delta t) \end{bmatrix} \tag{5}$$

If maneuvers are executed every Δt seconds, a desired relative station-keeping position $\mathbf{R}_{\mathrm{des}}^{\mathrm{LVLH}}$ can be achieved by issuing

maneuver commands equal to

$$\Delta\mathbf{v} = \Phi_{rv}^{-1}(\Delta t)\left\{\mathbf{R}_{\text{des}}^{\text{LVLH}} - \Phi_{rr}(\Delta t)\mathbf{R}_0^{\text{LVLH}}\right\} - \mathbf{V}_0^{\text{LVLH}} \tag{6}$$

However, the $\Delta\mathbf{v}$ that actually gets executed is

$$\Delta\mathbf{v} = \Phi_{rv}^{-1}(\Delta t)\left\{\mathbf{R}_{\text{des}}^{\text{LVLH}} - \Phi_{rr}(\Delta t)\hat{\mathbf{R}}_0^{\text{LVLH}}\right\} - \hat{\mathbf{V}}_0^{\text{LVLH}} + \boldsymbol{\varepsilon}_{\Delta\mathbf{v}} \tag{7}$$

where $\hat{\mathbf{R}}_0^{\text{LVLH}}$ and $\hat{\mathbf{V}}_0^{\text{LVLH}}$ are the current navigation filter estimates, and where $\boldsymbol{\varepsilon}_{\Delta\mathbf{v}}$ represents the maneuver execution error. Note that the position and velocity navigation errors are $\delta\mathbf{R}_0^{\text{LVLH}} = \hat{\mathbf{R}}_0^{\text{LVLH}} - \mathbf{R}_0^{\text{LVLH}}$ and $\delta\mathbf{V}_0^{\text{LVLH}} = \hat{\mathbf{V}}_0^{\text{LVLH}} - \mathbf{V}_0^{\text{LVLH}}$.

By substituting Eq. (7) into Eq. (1) and subtracting the desired station-keeping position we can determine $\Delta\mathbf{r}_{\text{sk}}$, the *station-keeping position error*:

$$\Delta\mathbf{r}_{\text{sk}} = \mathbf{R}^{\text{LVLH}}(t_0 + \Delta t) - \mathbf{R}_{\text{des}}^{\text{LVLH}} = \Phi_{rr}(\Delta t)\delta\mathbf{R}_0^{\text{LVLH}} + \Phi_{rv}(\Delta t)\left\{\delta\mathbf{V}_0^{\text{LVLH}} + \boldsymbol{\varepsilon}_{\Delta\mathbf{v}}\right\} + \int_0^{\Delta t}\Phi_{rv}(\tau)\mathbf{a}_d\,\mathrm{d}\tau \tag{8}$$

Using this equation, two special cases are examined. In one case we assume that the time between maneuvers is small relative to the orbit period $\Delta t \ll P_{\text{orb}}$. In the second case we assume that the time is greater than or equal to the orbit period $\Delta t \geq P_{\text{orb}}$.

$\Delta t \geq$ Orbital Period

For $\Delta t \geq P_{\text{orb}}$ the station-keeping position error $\Delta\mathbf{r}_{\text{sk}}$ is dominated by the downrange growth terms in the transition matrices. Substituting Eqs. (2) and (3) into Eq. (8) and keeping only the downrange growth terms produces

$$\Delta r_{\text{sk}} \approx -6\omega_{\text{orb}}\delta x_0\Delta t - 3\delta\dot{y}_0\Delta t - 3\varepsilon_{\Delta\mathbf{v}_y}\Delta t - \int_o^{\Delta t} 3a_{d_y}\tau\,\mathrm{d}\tau \tag{9}$$

where δx_0 is the altitude navigation error, $\delta\dot{y}_0$ is the downrange velocity navigation error, and $\varepsilon_{\Delta\mathbf{v}_y}$ is the downrange component of the maneuver execution error. Notice that the first two terms in this expression can conveniently be written in terms of the relative semimajor axis navigation error δa_0 where

$$\delta a_0 = \frac{2\delta\dot{y}_0}{\omega_{\text{orb}}} + 4\delta x_0 \tag{10}$$

Thus, we have

$$\Delta r_{\text{sk}} \approx \frac{3\omega_{\text{orb}}\delta a_0}{2}\Delta t - 3\varepsilon_{\Delta\mathbf{v}_y}\Delta t - \int_o^{\Delta t} 3a_{d_y}\tau\,\mathrm{d}\tau \tag{11}$$

If we assume that a_{d_y} is a zero-mean Gaussian random variable with $E[a_{d_y}^2] = Q\delta(t)$ where Q is the *strength* of the accelerations and $\delta(t)$ is a Dirac delta function, we can determine an approximate expression for the standard deviation of the station-keeping position error σ_{sk} by squaring Eq. (11) and taking the expected value. This produces

$$\sigma_{\text{sk}} \approx \sqrt{\left(\frac{3\omega_{\text{orb}}\Delta T}{2}\right)^2\sigma_{\delta a}^2 + 9\Delta t^2\sigma_{\varepsilon_{\Delta v}}^2 + 3\Delta t^3 Q} \tag{12}$$

where $\sigma_{\delta a}^2$ is the variance of the relative semimajor axis navigation error, $\sigma_{\varepsilon_{\Delta v}}^2$ is the variance of the maneuver execution error, and the correlation between navigation errors, maneuver execution errors, and random disturbances is assumed to be zero. Notice that the strength of the random accelerations, Q, has units of m^2/s^3. A more common measure of the effect of random accelerations is the level of downrange error per orbital period $\dot{D}$, induced by the unmodeled acceleration. When the only source of error is random acceleration, Eq. (12) can be used to show that the relationship between $\dot{D}$ and Q is simply

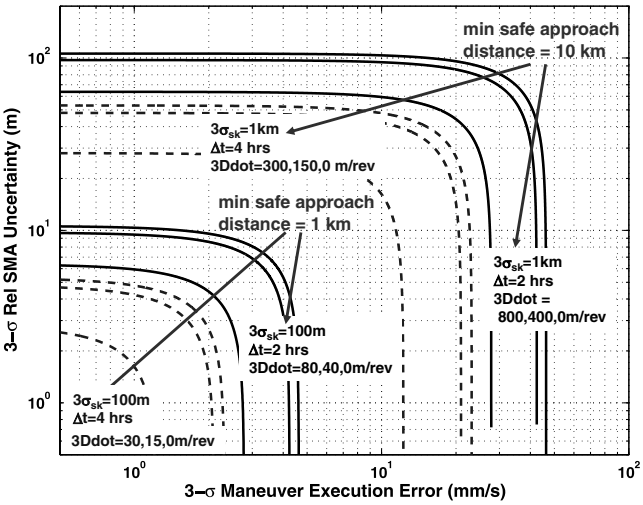

Fig. 3 Data for minimum ground-controlled closest-approach distances equal to 10 and 1 km ($f = 10\%$) are shown as a function of relative semimajor axis (SMA) navigation error, maneuver execution error, modeling error, and time between maneuvers when $\Delta t \geq P_{\text{orb}}$.

$$\dot{D}^2 = 3P_{\text{orb}}^3 Q \tag{13}$$

This expression is used to replace Q in Eq. (12) to produce

$$\sigma_{\text{sk}} \approx \sqrt{\left(\frac{3\pi\Delta T}{P_{\text{orb}}}\right)^2\sigma_{\delta a}^2 + 9\Delta t^2\sigma_{\varepsilon_{\Delta v}}^2 + \left(\frac{\Delta t}{P_{\text{orb}}}\right)^3\dot{D}^2} \tag{14}$$

This is an analytic expression for the standard deviation of the station-keeping dispersions, when $\Delta t \geq P_{\text{orb}}$, as a function of four key parameters—navigation error, maneuver execution error, unmodeled disturbances, and the time between maneuvers. Specific examples of this equation are plotted in Fig. 3. For $f = 10\%$ and $\Delta t = 2$ h, a minimum ground-controlled closest approach of 10 km ($3\sigma_{\text{sk}} = 1$ km) requires maneuver execution errors on the order of 30–50 mm/s and relative semimajor axis navigation errors on the order of 50–100 m. Higher maneuver accuracy and navigation accuracy are required as the level of disturbances is increased or as the time between maneuvers is increased. The data for a ground-controlled closest approach of 1 km ($3\sigma_{\text{sk}} = 100$ m) is also shown.

$\Delta t \ll$ Orbital Period

The next case to be considered is when the time between maneuvers is small relative to the orbit period $\Delta t \ll P_{\text{orb}}$. Small angle assumptions can be used in Eqs. (2) and (3) and substituted into Eq. (8). The result is

$$\Delta\mathbf{r}_{\text{sk}} \approx \delta\mathbf{R}_0^{\text{LVLH}} + \left\{\delta\mathbf{V}_0^{\text{LVLH}} + \boldsymbol{\varepsilon}_{\Delta\mathbf{v}}\right\}\Delta t + \int_0^{\Delta t}\mathbf{a}_d\tau\,\mathrm{d}\tau \tag{15}$$

If we neglect the correlation between position and velocity errors and assume $\delta\mathbf{R}_0^{\text{LVLH}}$, $\delta\mathbf{V}_0^{\text{LVLH}}$, $\boldsymbol{\varepsilon}_{\Delta\mathbf{v}}$, and $\mathbf{a}_d$ are uncorrelated, the standard deviation of the magnitude of the station-keeping error is given by

$$\sigma_{\text{sk}} \approx \sqrt{\sigma_r^2 + \left(\sigma_v^2 + \sigma_{\varepsilon_{\Delta\mathbf{v}}}^2\right)\Delta t^2 + Q\Delta t^3} \tag{16}$$

This equation can be simplified further by noting that relative position and velocity navigation errors for spacecraft in near circular orbits are often related by [5] $\sigma_v \approx \omega_{\text{orb}}\sigma_r$. [When this is not true Eq. (16) should be used.] Using Eq. (13) to write Q in terms of $\dot{D}$ and noting that $\omega_{\text{orb}}\Delta T \ll 1$ produces

$$\sigma_{\text{sk}} \approx \sqrt{\sigma_r^2 + \sigma_{\varepsilon_{\Delta\mathbf{v}}}^2\Delta t^2 + \frac{1}{3}\left(\frac{\Delta t}{P_{\text{orb}}}\right)^3\dot{D}^2} \tag{17}$$

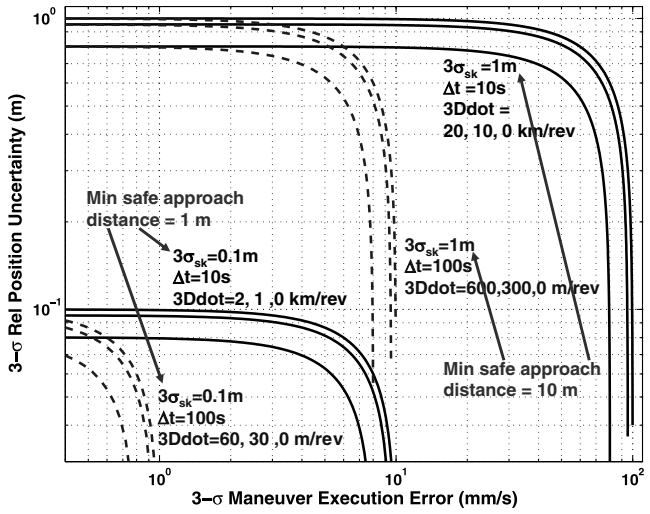

Fig. 4 Data for minimum ground-controlled closest-approach distances equal to 10 and 1 m ($f = 10\%$) are shown as a function of relative position navigation error, maneuver execution error, modeling error, and time between maneuvers when $\Delta t \ll P_{\text{orb}}$.

This is an analytic expression for the standard deviation of the station-keeping dispersions, when $\Delta t \ll P_{\text{orb}}$. Specific examples of this equation are plotted in Fig. 4. For $f = 10\%$ and $\Delta t = 10$ s, a minimum ground-controlled closest approach of 10 m ($3\sigma_{\text{sk}} = 1$ m) requires maneuver execution errors on the order of 80–100 mm/s and relative position navigation errors on the order of 80–100 cm. Higher maneuver accuracy and navigation accuracy are required as the level of disturbances is increased or as the time between maneuvers is increased. The data for a ground-controlled closest approach of 1 m ($3\sigma_{\text{sk}} = 0.1$ m) are also shown.

Modeling for Detailed Analysis

Next, a detailed analysis of a ground-controlled station-keeping problem will be conducted. The models for the detailed analysis include chaser and RSO translation dynamics, a simple model for chaser attitude dynamics, a lidar sensor model for relative navigation, a thruster model for position control, a Kalman filter for navigation, and a feedback control law for translational control. It is assumed that the chaser is in the vicinity of the RSO and requires only small brief maneuvers that can be modeled impulsively.

The *truth* model has a 28-dimensional state vector defined by

$$\mathbf{x} = (\mathbf{x}_o, \mathbf{x}_c, \mathbf{p})^T \tag{18}$$

where $\mathbf{x}_o$ is a six element *object* state, $\mathbf{x}_c$ is a six element *chaser* state, and $\mathbf{p}$ is a 16 element *parameter* state. The RSO and the chaser states consist of inertial position and velocity. The parameter states consist of sensor, actuator, and environment parameter errors including an attitude dispersion $\boldsymbol{\theta}_c^c$ from the nominal LVLH attitude $\bar{\mathbf{q}}_c^i$, lidar instrument misalignment error $\boldsymbol{\epsilon}_{\text{lidar}}$, lidar measurement bias error b_{lidar}, and actuator scale-factor error $f_{\Delta v}$, misalignment error $\boldsymbol{\epsilon}_{\Delta \mathbf{v}}$, and bias error $b_{\Delta v}$.

$$\mathbf{p} = \left(\boldsymbol{\theta}_c^c, \boldsymbol{\epsilon}_{\text{lidar}}, b_{\text{lidar}}, f_{\Delta v}, \boldsymbol{\epsilon}_{\Delta \mathbf{v}}, b_{\Delta v}\right)^T \tag{19}$$

These parameters are typically time varying biases with known time constants and modeled as first-order Markov processes.

Dynamics

The dynamics for the true state vector are given by

$$\dot{\mathbf{r}}_o^{\,i} = \mathbf{v}_o^i \tag{20}$$

$$\dot{\mathbf{v}}_o^{\,i} = \mathbf{F}^i_{\text{grav}_o}(\mathbf{r}_o^i)/m_o + \mathbf{a}_o \tag{21}$$

$$\dot{\mathbf{r}}_c^{\,i} = \mathbf{v}_c^i \tag{22}$$

$$\dot{\mathbf{v}}_c^{\,i} = \mathbf{F}^i_{\text{grav}_c}(\mathbf{r}_c^i)/m_c + \mathbf{a}_c \tag{23}$$

$$\dot{p}_i = -\frac{p_i}{\tau_i} + w_{p_i}, \qquad i = 1, 2, 3, \ldots, 16 \tag{24}$$

where m_o and m_c are the resident space object and chaser masses. Impulsive maneuvers $\Delta \mathbf{v}^i_{\text{act}}$ are used to *correct* the chaser velocity.

$$\left(\mathbf{v}_c^i\right)^{+c} = \left(\mathbf{v}_c^i\right)^{-c} + \Delta \mathbf{v}^i_{\text{act}}\left(\Delta \hat{\mathbf{v}}^c_{\text{com}}, \bar{\mathbf{q}}_c^i, \boldsymbol{\theta}_c^c, f_{\Delta v}, \boldsymbol{\epsilon}_{\Delta \mathbf{v}}, b_{\Delta v}\right) \tag{25}$$

The model for $\Delta \mathbf{v}^i_{\text{act}}$ is defined in Eq. (26), and all parameters p_i are first-order Markov processes driven by white noise w_{p_i}.

The gravitational forces on the chaser and the object, $\mathbf{F}^i_{\text{grav}_c}$ and $\mathbf{F}^i_{\text{grav}_o}$, are point mass plus J_2 gravity models [6]. Additional random accelerations $\mathbf{a}_c$, $\mathbf{a}_o$ are used to represent modeling errors. The covariances of the disturbances are $E[\mathbf{a}_o(t)\mathbf{a}_o^T(t')] = E[\mathbf{a}_c(t)\mathbf{a}_c^T(t')] = Q_d\delta(t - t')$, and $E[\mathbf{a}_o(t)\mathbf{a}_c^T(t')] = 0$.

Actuator Model

The actuator model parameters are scale-factor uncertainty $\mathbf{f}_{\Delta v}$, alignment uncertainty $\boldsymbol{\epsilon}_{\Delta \mathbf{v}}$, and a bias uncertainty $\mathbf{b}_{\Delta v}$. In terms of these parameters and the attitude error $\boldsymbol{\theta}_c^c$, the impulsive Δv in Eq. (25) is given by

$$\Delta \mathbf{v}^i_{\text{act}}\left(\Delta \hat{\mathbf{v}}^c_{\text{com}}, \bar{q}_c^i, \boldsymbol{\theta}_c^c, f_{\Delta v}, \boldsymbol{\epsilon}_{\Delta \mathbf{v}}, b_{\Delta v}\right) = \mathcal{T}\left(\bar{\mathbf{q}}_c^i\right)\delta\mathcal{T}\left(\boldsymbol{\theta}_c^c\right)\delta\mathcal{T}(\boldsymbol{\epsilon}_{\Delta \mathbf{v}}) \times \{[I_{3\times 3} + \text{diag}(\mathbf{f}_{\Delta v})]\Delta \hat{\mathbf{v}}^c_{\text{com}} + \mathbf{b}_{\Delta v} + \Delta \mathbf{w}_{\Delta v}\} \tag{26}$$

where the actuator commands $\Delta \hat{\mathbf{v}}^c_{\text{com}}$ generated by the flight computer are given in Eq. (47), and the covariance of the actuation noise is given by $E[\Delta \mathbf{w}_{\Delta v}(t_j)\Delta \mathbf{w}^T_{\Delta v}(t_{j'})] = S_{\Delta w_{\Delta v}}(t_j)\delta_{jj'}$.

Sensor Models

The lidar instrument is used by the chaser to image and track the resident space object. The instrument provides line of sight and range information. The model contains an uncertainty in the alignment of the instrument with respect to the chaser frame $\boldsymbol{\epsilon}_{\text{lidar}}$.

The bearing measurements $\tilde{\mathbf{l}}^{\text{lidar}}$ are given by [7]

$$\tilde{\mathbf{l}}^{\text{lidar}} = \begin{bmatrix} l_x/l_z \\ l_y/l_z \end{bmatrix} + \boldsymbol{\nu}_{\text{lidar}} \tag{27}$$

where the relative position of the object, $\mathbf{l}^{\text{lidar}}_{\text{los}} = [l_x, l_y, l_z]^T$, in the lidar frame, is given by

$$\mathbf{l}^{\text{lidar}}_{\text{los}} = \delta\mathcal{T}(\boldsymbol{\epsilon}_{\text{lidar}})\bar{\mathcal{T}}^c_{\text{lidar}}\delta\mathcal{T}\left(\boldsymbol{\theta}_c^c\right)\mathcal{T}\left(\bar{\mathbf{q}}_c^i\right)\left(\mathbf{r}_o^i - \mathbf{r}_c^i\right) \tag{28}$$

The covariance of the measurement noise is $E[\boldsymbol{\nu}_{\text{lidar}}(t_k)\boldsymbol{\nu}^T_{\text{lidar}}(t_{k'})] = R_{\boldsymbol{\nu}_{\text{lidar}}}\delta_{kk'}$. The range measurement model is

$$\tilde{r}_{\text{lidar}} = |\mathbf{r}_o^i - \mathbf{r}_c^i| + b_{\text{lidar}} + \boldsymbol{\nu}_{\text{range}} \tag{29}$$

where b_{lidar} is an unknown bias and the covariance of the measurement noise $\boldsymbol{\nu}_{\text{range}}$ is $E[\boldsymbol{\nu}_{\text{range}}(t_k)\boldsymbol{\nu}^T_{\text{range}}(t_{k'})] = R_{\boldsymbol{\nu}_{\text{range}}}\delta_{kk'}$.

Navigation Algorithm

The navigation state *propagation* equations are given by

$$\dot{\hat{\mathbf{r}}}_o^{\,i} = \hat{\mathbf{v}}_o^i \tag{30}$$

$$\dot{\hat{\mathbf{v}}}_o^{\,i} = \hat{\mathbf{F}}^i_{\text{grav}_o}\left(\hat{\mathbf{r}}_o^i\right)/\hat{m}_o \tag{31}$$

$$\dot{\hat{\mathbf{r}}}_c^{\,i} = \hat{\mathbf{v}}_c^i \tag{32}$$

$$\dot{\hat{\mathbf{v}}}_c^{\,i} = \hat{\mathbf{F}}^i_{\text{grav}_c}\left(\hat{\mathbf{r}}^i_c\right)/\hat{m}_c \tag{33}$$

$$\dot{\hat{p}}_i = -\frac{\hat{p}_i}{\hat{\tau}_i}, \qquad i = 1, 2, 3, \ldots, 16 \tag{34}$$

The gravitational forces on the chaser and the object, $\hat{\mathbf{F}}^i_{\text{grav}_c}$ and $\hat{\mathbf{F}}^i_{\text{grav}_o}$, are point mass plus J_2 gravity models [6].

The navigation state covariance propagation equation is

$$\dot{\hat{P}} = \hat{F}_{\hat{x}}\hat{P} + \hat{P}\hat{F}^T_{\hat{x}} + \hat{S}_w \tag{35}$$

where the partial derivatives $\hat{F}_{\hat{x}}$ and the state process noise covariance $\hat{S}_w$ are given in Eqs. (A1–A5).

The navigation state *update* equation is

$$\hat{\mathbf{x}}_k^{\,+} = \hat{\mathbf{x}}_k^- + \hat{K}(t_k)\left[\tilde{\mathbf{z}}_k - \hat{\mathbf{h}}\left(\hat{\mathbf{x}}_k, t_k\right)\right] \tag{36}$$

where $\hat{\mathbf{h}}(\hat{\mathbf{x}}_k, t_k)$ is based on both Eqs. (27) and (29).

The navigation state covariance update equation is given by

$$\begin{aligned}\hat{P}(t_k^+) = {} & \left[I - \hat{K}(t_k)\hat{H}_{\hat{x}}(t_k)\right]\hat{P}\left(t_k^-\right)\left[I - \hat{K}(t_k)\hat{H}_{\hat{x}}(t_k)\right]^T \\ & + \hat{K}(t_k)\hat{R}_v(t_k)\hat{K}^T(t_k)\end{aligned} \tag{37}$$

where $\hat{K}(t_k)$ is the Kalman gain [8]. The measurement sensitivity matrice $\hat{H}_{\hat{x}}$ and the measurement covariance matrices $\hat{R}_v$ for the lidar are given in Eqs. (A6–A9).

Finally, when an impulsive maneuver Δv is used to correct the chaser velocity, a correction must be made to the navigation state

$$\left(\hat{\mathbf{v}}^i_c\right)^{+c} = \left(\hat{\mathbf{v}}^i_c\right)^{-c} + \Delta\hat{\mathbf{v}}^i_{\text{act}}\left(\Delta\hat{\mathbf{v}}^c_{\text{com}}, \bar{\mathbf{q}}^i_c, \hat{\boldsymbol{\theta}}^c_c, \hat{f}_{\Delta v}, \hat{\boldsymbol{\epsilon}}_{\Delta v}, \hat{b}_{\Delta v}\right) \tag{38}$$

where

$$\begin{aligned}&\Delta\hat{\mathbf{v}}^i_{\text{act}}\left(\Delta\hat{\mathbf{v}}^c_{\text{com}}, \bar{\mathbf{q}}^i_c, \hat{\boldsymbol{\theta}}^c_c, \hat{f}_{\Delta v}, \hat{\boldsymbol{\epsilon}}_{\Delta v}, \hat{b}_{\Delta v}\right) \\ &= \hat{\mathcal{T}}\left(\bar{\mathbf{q}}^c_i\right)\delta\hat{\mathcal{T}}\left(-\hat{\boldsymbol{\theta}}^c_c\right)\delta\hat{\mathcal{T}}\left(\hat{\boldsymbol{\epsilon}}_{\Delta v}\right)\left\{\left[I_{3\times3} + \text{diag}\left(\hat{\mathbf{f}}_{\Delta v}\right)\right]\Delta\hat{\mathbf{v}}^c_{\text{com}} + \hat{\mathbf{b}}_{\Delta v}\right\}\end{aligned} \tag{39}$$

The maneuver command $\Delta\hat{\mathbf{v}}^c_{\text{com}}$ is given in Eq. (47), and $\hat{\mathbf{f}}_{\Delta v}$, $\hat{\boldsymbol{\epsilon}}_{\Delta v}$, and $\hat{\mathbf{b}}_{\Delta v}$ are the flight computer values of actuator scale factor, misalignment, and bias. The actuation noise covariance due to (for example) actuator quantization error is simply

$$\hat{S}^{\text{quant}}_{\Delta w} = \text{diag}\left(\left[\sigma^2_{\text{quant}_x}, \sigma^2_{\text{quant}_y}, \sigma^2_{\text{quant}_z}\right]\right) \tag{40}$$

When a correction is made to the navigation state, a correction is also made to the navigation state covariance matrix

$$\hat{P}\left(t_j^{+c}\right) = \left[I + \hat{D}_{\hat{x}}(t_j)\right]\hat{P}\left(t_j^{-c}\right)\left[I + \hat{D}_{\hat{x}}(t_j)\right]^T + \hat{S}^{\text{quant}}_{\Delta w}(t_j) \tag{41}$$

where the partial derivative $\hat{D}_{\hat{x}}$ is given in Eqs. (A10) and (A11).

Translation Control

The maneuver targeting algorithm is based on the Clohessy–Wiltshire equations [9] and is referred to as the CW-targeting algorithm. In a LVLH coordinate frame, the CW equations can be written as

$$\begin{bmatrix}\hat{\mathbf{R}}^{\text{LVLH}}(t_0 + \Delta t) \\ \hat{\mathbf{V}}^{\text{LVLH}}(t_0 + \Delta t)\end{bmatrix} = \begin{bmatrix}\Phi_{rr}(\Delta t) & \Phi_{rv}(\Delta t) \\ \Phi_{vr}(\Delta t) & \Phi_{vv}(\Delta t)\end{bmatrix}\begin{bmatrix}\hat{\mathbf{R}}^{\text{LVLH}}(t_0) \\ \hat{\mathbf{V}}^{\text{LVLH}}(t_0)\end{bmatrix} \tag{42}$$

where

$$\hat{\mathbf{R}}^{\,\text{LVLH}}(t_0) = \hat{\mathcal{T}}^i_{\text{LVLH}}\left(\hat{\mathbf{r}}^i_c - \hat{\mathbf{r}}^i_o\right) \tag{43}$$

$$\hat{\mathbf{V}}^{\,\text{LVLH}}(t_0) = \hat{\mathcal{T}}^i_{\text{LVLH}}\left[\hat{\mathbf{v}}^i_c - \hat{\mathbf{v}}^i_o - \hat{\boldsymbol{\omega}}^i_{\text{orb}} \times \left(\hat{\mathbf{r}}^i_c - \hat{\mathbf{r}}^i_o\right)\right] \tag{44}$$

$$\hat{\boldsymbol{\omega}}^{\,i}_{\text{orb}} = \hat{\mathbf{v}}^i_o \times \hat{\mathbf{r}}^i_o / \|\hat{\mathbf{r}}^i_o\|^2 \tag{45}$$

To achieve a desired relative position $\hat{\mathbf{R}}^{\text{LVLH}}_{\text{des}}$ at time $t_0 + \Delta t$, the required $\Delta\mathbf{v}$ at time t_0 is

$$\begin{aligned}\Delta\hat{\mathbf{v}}^{\text{LVLH}}_{\text{req}} = {} & \Phi^{-1}_{rv}(\Delta t)\left[\hat{\mathbf{R}}^{\text{LVLH}}_{\text{des}} - \Phi_{rr}(\Delta t)\hat{\mathcal{T}}^i_{\text{LVLH}}\left(\hat{\mathbf{r}}^i_c - \hat{\mathbf{r}}^i_o\right)\right] \\ & - \hat{\mathcal{T}}^i_{\text{LVLH}}\left[\hat{\mathbf{v}}^i_c - \hat{\mathbf{v}}^i_o - \hat{\boldsymbol{\omega}}^i_{\text{orb}} \times \left(\hat{\mathbf{r}}^i_c - \hat{\mathbf{r}}^i_o\right)\right]\end{aligned} \tag{46}$$

The $\Delta\mathbf{v}$ command to the actuators is the required $\Delta\mathbf{v}$ given above, transformed to the chaser frame with compensation for known actuator errors:

$$\begin{aligned}&\Delta\hat{\mathbf{v}}^c_{\text{com}} \\ &= \delta\hat{\mathcal{T}}\left(-\hat{\boldsymbol{\epsilon}}_{\Delta v}\right)\left[I_{3\times3} - \text{diag}\left(\hat{\mathbf{f}}_{\Delta v}\right)\right]\delta\mathcal{T}\left(\hat{\boldsymbol{\theta}}^c_c\right)\hat{\mathcal{T}}\left(\bar{\mathbf{q}}^i_c\right)\hat{\mathcal{T}}^{\text{LVLH}}_i\Delta\hat{\mathbf{v}}^{\text{LVLH}}_{\text{req}} \\ &- \hat{\mathbf{b}}_{\Delta v}\end{aligned} \tag{47}$$

Detailed Analysis Results

The detailed analysis of a ground-controlled station-keeping problem is conducted using linear covariance (LinCov) techniques [3] which produce the same statistical results as a Monte Carlo simulation without doing hundreds or thousands of simulations. This provides the capability to study the effects of many GNC parameters in a short period of time.

The LinCov analysis tool is derived from the rendezvous GNC Monte Carlo program shown in Fig. 5 which is in turn derived from the math models in the section Modeling for Detailed Analysis. In the Monte Carlo simulation, white noise processes and flight computer actuator commands drive truth models which in turn generate the true state $\mathbf{x}$ of the system along with simulated sensor measurements. A navigation algorithm processes the sensor data and produces a navigation state $\hat{\mathbf{x}}$ and a navigation state error covariance $\hat{P}$. The navigation state is used by control functions of the flight computer to generate the actuator commands. The key variables are the *true dispersions* from the reference trajectory, $\delta\mathbf{x} = \mathbf{x} - \bar{\mathbf{x}}$, the *navigation dispersions* from the reference trajectory $\delta\hat{\mathbf{x}} = \hat{\mathbf{x}} - \bar{\mathbf{x}}$, and the *true navigation errors*, $\delta\mathbf{e} = \delta\hat{\mathbf{x}} - M_x\delta\mathbf{x}$.

In a Monte Carlo program, the covariance of the dispersions and navigation errors are determined by collecting and compiling the results of N simulations.

$$\begin{aligned}D_{\text{true}} &\approx \frac{1}{N-1}\sum_{i=1}^{N}\delta\mathbf{x}\delta\mathbf{x}^T, \qquad D_{\text{nav}} \approx \frac{1}{N-1}\sum_{i=1}^{N}\delta\hat{\mathbf{x}}\delta\hat{\mathbf{x}}^T \\ P_{\text{true}} &\approx \frac{1}{N-1}\sum_{i=1}^{N}\delta\mathbf{e}\delta\mathbf{e}^T\end{aligned} \tag{48}$$

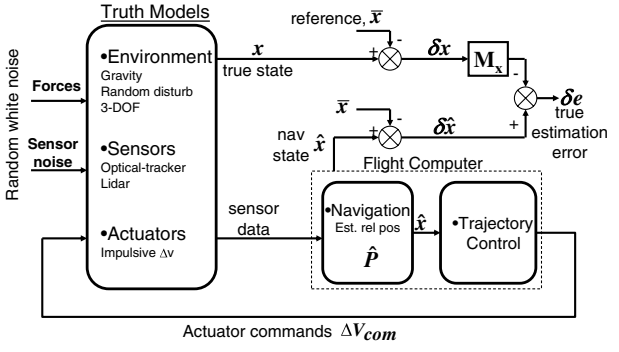

Fig. 5 A generic Monte Carlo Simulation for GNC analysis.

Table 1 Nominal trajectory, disturbances, sensor, and actuator parameters

Nominal initial condition error 3-σ		
Attitude dispersion and knowledge error	Per axis	1.0 mrad
Position, velocity dispersion/knowledge error	Per axis	10% of separation, pos error $\cdot\ \omega_{\text{orb}}$
Nominal unmodeled disturbances 3-σ		
Translational disturbances	Per axis	varied (see text)
Nominal sensor error 3-σ		
Lidar errors	Misalignment	1.0 mrad/axis
	Angle random	1.0 mrad
	Range random	0.1% of range
	Range bias	0.1% of range
Nominal actuator error 3-σ		
Maneuver execution error	Directional	1 mrad/axis
	Scale factor	1000 ppm
	Random	Varied (see text)
	Bias	Varied (see text)

Table 2 Numerical and analytical data for station-keeping dispersions $3\sigma_{\text{sk}}$ in a 2-h Martian orbit when $\Delta t \geq P_{\text{orb}}$

Case	Δt, min	$3\sigma_{\Delta v}$, mm/s	$3\dot{D}$, m/orbit	$3\sqrt{Q}$, m/s/$\sqrt{s}$	$3\sigma_{\delta a}$, m	LinCov $3\sigma_{\text{sk}}$, m	Eq. (14) $3\sigma_{\text{sk}}$, m	Error, %
1	100	30	0	0	3.2	440–580	540	7%
2	100	9	900	8.5×10^{-4}	47	880–1410	798	43%
3	100	3	0	0	1.1	43–59	54	8%
4	100	0.9	90	8.5×10^{-5}	6.5	92–142	86	40%
5	200	30	0	0	0.5	600–1050	1080	3%
6	200	9	900	8.5×10^{-4}	47	110–2450	2102	14%
7	200	3	0	0	0.95	55–105	109	4%
8	200	0.9	90	8.5×10^{-5}	6.5	110–253	196	22%

The covariance of trajectory dispersions and navigation errors are of primary interest.

In a linear covariance approach, the covariances in Eq. (48) are generated in a single simulation by directly propagating, updating, and correcting an *augmented* state covariance matrix [3]. This technique will be used to determine the covariance of station-keeping dispersions and navigation errors. Numerical results will be compared to the analytical results in Eqs. (14) and (17).

The error sources included in the analysis are summarized in Table 1. Numerical values are given for those that were held constant throughout the analysis. The remaining values will be specified as each case is discussed in the sections below.

Mars Orbit Rendezvous for Sample Return, $\Delta t \geq P_{\text{orb}}$

In this case, considered ground-controlled station keeping at 10 and 1 km in a 2-h Martian orbit is considered. Maneuvers are computed and uplinked every 100–200 min. Lidar measurements are taken every 60 s and downlinked to the ground. The round-trip light-travel time is assumed to be 30 min, and the LinCov tool is used to determine the position dispersion σ_{sk} around the station-keeping position. Table 2 shows the numerical results and the analytical results. The time between maneuvers in cases 1–4 is 100 min. The time between maneuvers in cases 5–8 is 200 min. All cases show good agreement between the numerical and analytical results except for cases 2 and 4 where the analytic station-keeping dispersions are low. This is believed to be due to the fact that Eq. (14) ignores cyclical error terms which are still significant when $\Delta t = 100 \approx P_{\text{orb}}$. Figures 6 and 7 show the 3-σ position dispersion and navigation error and the 3-σ relative semimajor axis dispersion and navigation error. The analytical prediction for the position dispersion is also shown (540 m for case 1 and 794 for case 2)

Low Lunar Orbit Rendezvous, $\Delta t \geq P_{\text{orb}}$

In this case, ground-controlled station keeping at 10 and 1 km in a 2-h lunar orbit is considered. Maneuvers are computed and uplinked every 100–200 min. The main difference between this scenario and the Mars sample return scenario is that the navigation error at the time maneuvers are computed is smaller for the lunar orbit because of the shorter light-travel time to the ground. Thus, the lunar results are nearly identical to the results shown in Table 2 when the lunar orbit period is 2 h and maneuvers are every 100–200 min. This is also reflected in Eq. (14) which is dependent on orbit period and independent of the gravitational constant.

Low Lunar Orbit Rendezvous, $\Delta t \ll P_{\text{orb}}$

This scenario considers ground-controlled station keeping at 10 and 1 m in a 2-h lunar orbit. Lidar measurements are taken every 1 s and downlinked to the ground. At lunar distances, the round-trip light-travel time is approximately 2.6 s and is conservatively assumed to be 3 s for this analysis. Linear covariance analysis is used

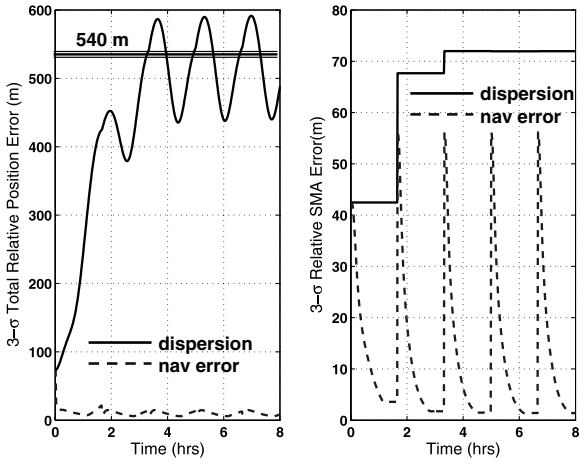

Fig. 6 3-σ position dispersion and navigation error for case 1. The analytical prediction for the position dispersion is 540 m.

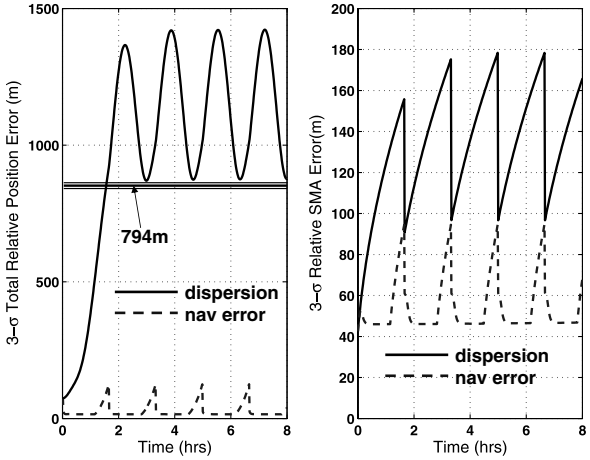

Fig. 7 3-σ position dispersion and navigation error for case 2. The analytical prediction for the position dispersion is 794 m.

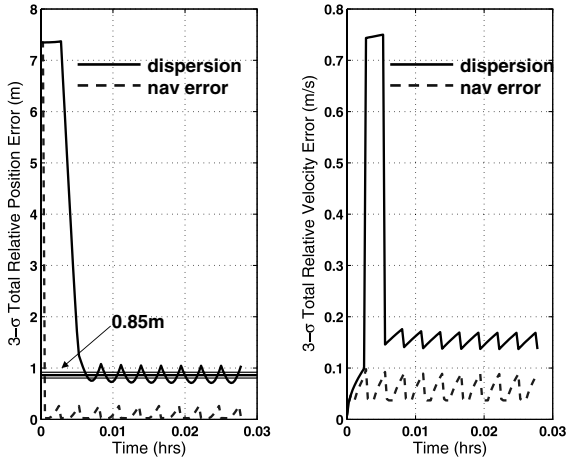

Fig. 8 3-σ position dispersion and navigation error for case 10. The analytical prediction for the position dispersion is 0.8 m.

to determine the position dispersion σ_{sk} around the station-keeping position. Table 3 shows the numerical results and the analytical results. The time between maneuvers in cases 5–8 is 10 s. The time between maneuvers in cases 9–12 is 100 s. All cases show good agreement between the numerical and analytical results.

Figure 8 shows the 3-σ position dispersion and navigation error and the 3-σ relative semimajor axis dispersion and navigation error. The analytical prediction for the position dispersion is also shown (0.8 m).

Geosynchronous Orbit, $\Delta t \ll P_{orb}$

This scenario considers ground-controlled station keeping at 10 and 1 m in a 24 h Earth orbit. Lidar measurements are taken every 1 s and downlinked to the ground. At GEO distances the round-trip light-travel time is approximately 2.81 msec and is conservatively assumed to be 3 msec. Linear covariance analysis is used to determine the position dispersion σ_{sk} around the station-keeping position. Although this scenario seems very different than the previous scenario, the results are very similar, especially for the low-disturbance cases. In fact, Eqs. (16) and (17) show that for small disturbances, the motion is fundamentally rectilinear and independent of P_{orb} when $\Delta t \ll P_{orb}$. The linear covariance results in Table 4 clearly show this. Table 4 shows the numerical results and the analytical results. The time between maneuvers in cases 17–20 is 10 s, and the time between maneuvers in cases 21–24 is 100 s. All cases show good agreement between the numerical and analytical results.

Figure 9 shows the 3-σ position dispersion and navigation error and the 3-σ relative semimajor axis dispersion and navigation error for case 24. The analytical prediction for the position dispersion is also shown (0.085 m)

Conclusions

Analytic expressions that estimate the relative position dispersion of two spacecraft being controlled from the ground have been derived. The dispersion is a function of navigation error, maneuver

Table 3 Numerical and analytic data for station-keeping dispersions $3\sigma_{sk}$ in a 2-h lunar orbit when $\Delta t \ll P_{orb}$

Case	Δt, s	$3\sigma_{\Delta v}$, mm/s	$3\dot{D}$, m/orbit	$3\sqrt{Q}$, m/s/$\sqrt{s}$	$3\sigma_{\delta r}$, m	$3\sigma_{\delta v}$, mm/s	LinCov $3\sigma_{sk}$, m	Eqs. (16) or (17) $3\sigma_{sk}$, m	Error, %
9	10	90	0	0	0.025	5.0	0.78–1.08	0.90	25%
10	10	60	20,000	1.9×10^{-2}	0.025	4.0	0.72–1.04	0.85	18%
11	10	9	0	0	0.023	4.0	0.08–0.11	0.093	15%
12	10	6	2000	1.9×10^{-3}	0.021	3.5	0.07–0.11	0.088	20%
13	100	9	0	0	0.020	0.5	0.9-1.25	0.95	24%
14	100	6	600	5.7×10^{-4}	0.021	2.5	0.72–1.04	0.86	17%
15	100	0.9	0	0	0.002	0.5	0.09–0.12	0.09	25%
16	100	0.6	60	5.7×10^{-5}	0.002	0.2	0.07–0.1	0.085	15%

Table 4 Numerical and analytic data for station-keeping dispersions $3\sigma_{sk}$ in a 24-h Earth orbit when $\Delta t \ll P_{orb}$

Case	Δt, s	$3\sigma_{\Delta v}$, mm/s	$3\dot{D}$, m/orbit	$3\sqrt{Q}$, m/s/$\sqrt{s}$	$3\sigma_{\delta r}$, m	$3\sigma_{\delta v}$, mm/s	LinCov $3\sigma_{sk}$, m	Eqs. (16) or (17) $3\sigma_{sk}$, m	Error, %
17	10	90	0	0	0.025	5.0	0.78–1.08	0.90	25%
18	10	60	800,000	1.8×10^{-2}	0.025	3.5	0.70–0.98	0.90	8%
19	10	9	0	0	0.023	4.0	0.08–0.11	0.093	15%
20	10	6	80,000	1.8×10^{-3}	0.020	3.5	0.065–0.095	0.089	9%
21	100	9	0	0	0.020	0.5	0.9–1.25	0.95	24%
22	100	6	25,000	5.7×10^{-4}	0.022	2.5	0.72–1.05	0.82	22%
23	100	0.9	0	0	0.002	0.5	0.09–0.12	0.09	25%
24	100	0.6	2500	5.7×10^{-5}	0.02	0.2	0.07–0.1	0.085	15%

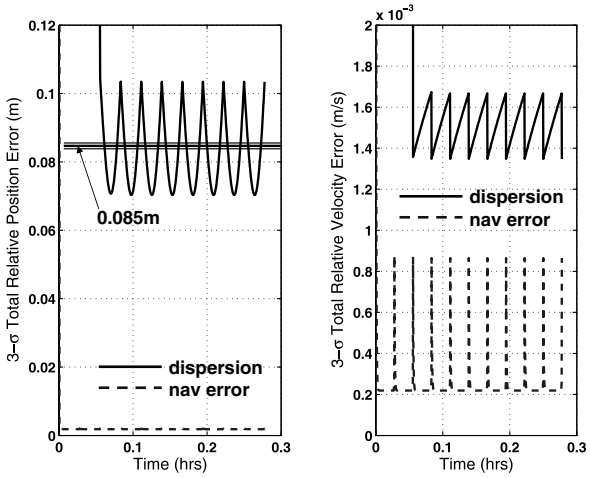

Fig. 9 3-σ position dispersion and navigation error for case 24. The analytical prediction for the position dispersion is 0.085 m.

execution error, environment modeling error, and the time between successive maneuvers. Detailed linear covariance analysis demonstrated that the analytic expressions are accurate to approximately $\pm 25\%$. A multiplier based on acceptable safety and risk levels can be applied to the relative dispersion to determine a minimum ground-controlled safe-approach distance.

For low Mars orbit rendezvous missions with maneuvers every 100–200 min, analysis shows that ground controllers can safely maintain separation distances of 10 km provided that maneuver accuracies are less than 10–40 mm/s, relative semimajor axis navigation errors are less than 30–80 m, and environment modeling errors are less 150–800 m/orbit. If 1 km separation distances are desired, the above requirements must be tightened by an order of magnitude. The requirements for 2-h low lunar orbits are nearly identical to the Mars orbit requirements.

For low lunar orbit and GEO orbit rendezvous missions with maneuvers every 10 s, ground controllers can safely maintain separation distances of 10 m when maneuver accuracies are less than 80–90 mm/s, relative position navigation errors are less than 0.8–0.9 m, and modeling errors are less than 10–20 km/orbit. When the time between maneuvers is increased to 100 s, maneuver accuracies and modeling errors must be improved to 8–9 mm/s, and 300–600 m/orbit, respectively. If 1 m separation distances are desired, all requirements must be tightened by an order of magnitude.

Appendix A: Matrix Partial Derivatives

The propagation of the navigation state $\dot{\hat{\mathbf{x}}} = \hat{\mathbf{f}}(\hat{\mathbf{x}}, \hat{\mathbf{u}}, \tilde{\mathbf{y}})$ is accomplished using Eqs. (30–34). The propagation of the navigation state covariance matrix in Eq. (35) is accomplished using the following partial derivatives and the state process noise covariance:

$$\hat{S}_w = \begin{bmatrix} \hat{S}_{w_o} & 0_{6\times6} & 0_{6\times16} \\ 0_{6\times6} & \hat{S}_{w_c} & 0_{6\times16} \\ 0_{16\times6} & 0_{16\times6} & -\mathrm{diag}([\hat{\sigma}^2_{p_1}, \hat{\sigma}^2_{p_2}, \ldots, \hat{\sigma}^2_{p_{16}}]) \end{bmatrix} \tag{A1}$$

$$\hat{F}_{\hat{x}} = \frac{\partial \dot{\hat{\mathbf{f}}}}{\partial \hat{\mathbf{x}}} = \begin{bmatrix} \hat{F}_{\hat{x}_o} & 0_{6\times6} & 0_{6\times16} \\ 0_{6\times6} & \hat{F}_{\hat{x}_c} & 0_{6\times16} \\ 0_{16\times6} & 0_{16\times6} & -\mathrm{diag}\left(\left[\frac{1}{\hat{\tau}_1}, \frac{1}{\hat{\tau}_2}, \ldots, \frac{1}{\hat{\tau}_{16}}\right]\right) \end{bmatrix} \tag{A2}$$

where

$$\hat{S}_{w_o} = \begin{bmatrix} 0_{3\times3} & 0_{3\times3} \\ 0_{3\times3} & \hat{Q}_d \end{bmatrix}, \qquad \hat{S}_{w_c} = \begin{bmatrix} 0_{3\times3} & 0_{3\times3} \\ 0_{3\times3} & \hat{Q}_d \end{bmatrix} \tag{A3}$$

$$\hat{F}_{\hat{x}_o} = \begin{bmatrix} 0_{3\times3} & I_{3\times3} \\ \hat{m}_o^{-1}\partial \mathbf{F}^i_{\mathrm{grav}_o}/\partial \hat{\mathbf{r}}^i_o & 0_{3\times3} \end{bmatrix} \tag{A4}$$

$$\hat{F}_{\hat{x}_c} = \begin{bmatrix} 0_{3\times3} & I_{3\times3} \\ \hat{m}_c^{-1}\partial \mathbf{F}^i_{\mathrm{grav}_c}/\partial \hat{\mathbf{r}}^i_c & 0_{3\times3} \end{bmatrix} \tag{A5}$$

The line-of-sight measurement sensitivity matrix for the lidar [7] is given by

$$\hat{H}^{\mathrm{lidar}}_{\hat{x}} = \begin{bmatrix} 1/\hat{l}_z & 0 & -\hat{l}_x/\hat{l}_z^2 \\ 0 & 1/\hat{l}_z & -\hat{l}_y/\hat{l}_z^2 \end{bmatrix} \frac{\partial \hat{\mathbf{l}}^{\mathrm{lidar}}_{\mathrm{los}}}{\partial \hat{\mathbf{x}}} \tag{A6}$$

where

$$\frac{\partial \hat{\mathbf{l}}^{\mathrm{lidar}}_{\mathrm{los}}}{\partial \hat{\mathbf{x}}} = \left[\hat{\mathcal{T}}^i_{\mathrm{lidar}}, 0_{3\times3}, -\hat{\mathcal{T}}^i_{\mathrm{lidar}}, 0_{3\times3}, \hat{\mathcal{T}}^c_{\mathrm{lidar}}\left[\left(\hat{\mathbf{r}}^c_o - \hat{\mathbf{r}}^c_c\right)\times\right],\right.$$
$$\left. 0_{3\times3}, \left[\left(\hat{\mathbf{r}}^{\mathrm{lidar}}_o - \hat{\mathbf{r}}^{\mathrm{lidar}}_c\right)\times\right], 0_{3\times3}, 0_{3\times3}, 0_{3\times3}, 0\right] \tag{A7}$$

The range measurement sensitivity for the lidar is

$$\hat{H}^{\mathrm{lidar}}_{\hat{x}} = \left[\left(\hat{i}^i_{\mathrm{rel}}\right)^T, 0_{1\times3}, -\left(\hat{i}^i_{\mathrm{rel}}\right)^T, 0_{1\times3}, 0_{1\times15}, 1\right] \tag{A8}$$

where $\hat{i}^i_{\mathrm{rel}} = (\hat{\mathbf{r}}^i_o - \hat{\mathbf{r}}^i_c)/|\hat{\mathbf{r}}^i_o - \hat{\mathbf{r}}^i_c|$.

The flight computer's value of the lidar angle measurement covariance is

$$\hat{R}^{\mathrm{lidar}}_v = \mathrm{diag}([\sigma^2_{\mathrm{lidar}_x}, \sigma^2_{\mathrm{lidar}_y}]) \tag{A9}$$

The correction of the navigation state covariance matrix in Eq. (41) is accomplished using the following partial derivative:

$$\hat{D}_{\hat{x}} = \begin{bmatrix} 0_{6\times6} & 0_{6\times6} & 0_{6\times16} \\ 0_{6\times6} & 0_{6\times6} & \hat{D}_{\hat{x}_p} \\ 0_{16\times6} & 0_{16\times6} & 0_{16\times16} \end{bmatrix} \tag{A10}$$

where

$$\hat{D}_{\hat{x}_p} = \begin{bmatrix} 0_{3\times3} & 0_{3\times3} & 0_{3\times3} & 0_{3\times3} & 0_{3\times3} & 0 \\ \partial \Delta \hat{\mathbf{v}}^i_{\mathrm{act}}/\partial \hat{\theta}^c_c & 0_{3\times3} & \partial \Delta \hat{\mathbf{v}}^i_{\mathrm{act}}/\partial \hat{\mathbf{f}}_{\Delta v} & \partial \Delta \hat{\mathbf{v}}^i_{\mathrm{act}}/\partial \hat{\epsilon}_{\Delta v} & \partial \Delta \hat{\mathbf{v}}^i_{\mathrm{act}}/\partial \hat{\mathbf{b}}_{\Delta v} & 0 \end{bmatrix} \tag{A11}$$

References

[1] Fehse, W., *Automated Rendezvous and Docking of Spacecraft*, Cambridge Univ. Press, New York, 2003, pp. 441–467.

[2] Zimpher, D., Kachmar, P., and Touhy, S., "Autonomous Rendezvous, Capture and In-Space Assembly: Past, Present, and Future," AIAA Paper 2005-2523, Jan. 2005.

[3] Geller, D. K., "Linear Covariance Techniques for Orbital Rendezvous Analysis and Autonomous On-Board Mission Planning," *Journal of Guidance, Control, and Dynamics*, Vol. 29, No. 6, 2006, pp. 1404–1414.

[4] Clohessy, W. H., and Wiltshire, R. S., "Terminal Guidance System for Satellite Rendezvous," *Journal of the Aerospace Sciences*, Vol. 27, No. 9, 1960, pp. 653–658.

[5] Chari, R., "Autonomous Orbital Rendezvous Using Angles-Only Navigation," M.S. Thesis, MIT, Cambridge, MA, May 2001, pp. 69–73.

[6] Kaplan, M. H., *Modern Spacecraft Dynamics and Control*, Wiley, New York, 1976, pp. 343–370.

[7] Pittelkau, M. E., "Rotation Vector in Attitude Estimation," *Journal of Guidance, Control, and Dynamics*, Vol. 26, No. 6, 2003, pp. 855–860.

[8] Maybeck, P. S., "Stochastic Models, Estimation, and Control," *Academic Press*, New York, 1979, p. 217.

[9] Vallado, D. A., *Fundamentals of Astrodynamics and Applications*, McGraw–Hill, New York, 1997, pp. 343–366.